J Mater Sci (2007) 42:10254–10274
DOI 10.1007/s10853-006-1199-9

Modelling of effects of ultrastructural morphology on the hygroelastic properties of wood fibres

R. Cristian Neagu · E. Kristofer Gamstedt

Received: 23 August 2006 / Accepted: 31 October 2006 / Published online: 5 September 2007

Abstract Wood fibres constitute the structural framework of e.g. wood, paper, board and composites, where stiffness and dimensional stability are of importance. An analytical modelling approach has been used for prediction of hygroelastic response, and assessment of the stresses in thick-walled cylinder models of wood fibres. A wood fibre was idealised as a multilayered hollow cylinder made of orthotropic material with helical orientation. The hygroelastic response of the layered assembly due to axisymmetric loading and moisture content changes was obtained by solving the corresponding boundary value problem of elasticity. A simple solution scheme based on the state space approach and the transfer matrix method was employed. This was combined with an analytical ultrastructural homogenisation method, used to link hygroelastic properties of constituent wood polymers to properties of each layer. Predicted hygroelastic response captured experimentally measured behaviour. Fibres that were constrained not to twist showed a stiffer response than fibres allowed twisting under uniaxial loading. It was also shown that the ultrastructure, i.e. the microfibril angle, will control the hygroexpansion in the same way as it controls the compliance of the cell wall. Qualitative failure trends comparable with experimental observations could be established with stress analysis and a simple plane-stress failure criterion.

R. C. Neagu (✉) · E. K. Gamstedt
New Materials and Composites, STFI-Packforsk AB, Box 5604, Stockholm 114 86, Sweden
e-mail: cristian.neagu@stfi.se

E. K. Gamstedt
e-mail: kristofer@hallf.kth.se

E. K. Gamstedt
KTH Solid Mechanics, School of Engineering Science, Royal Institute of Technology (KTH), Osquars backe 1, Stockholm 100 44, Sweden
e-mail: kristofer@hallf.kth.se

Introduction

In contrast to man-made fibres, wood fibres are renewable, biodegradable, recyclable, nonabrasive to processing equipment, can be incinerated and show less concern with safety and health. These factors combined with good specific properties and low cost make wood fibres an appealing alternative to e.g. glass fibres in engineering polymer composites. Wood fibre composites remain relatively novel materials, yet to reach their full potential. A long-term ambition is to tailor the nano- and microstructure of the composite in order to obtain optimal material performance. It is therefore desirable to develop efficient methods for materials development to assess the wood fibre ultrastructure and its influence on the mechanical efficiency of wood fibres in composites. The term 'ultrastructure' defines the extreme-fine structure of the cell wall resolvable with electron microscopy.

It is possible to study the relation between cell-wall structure on nano and micron scales and fibre properties, to gain increased understanding of the mechanical behaviour of wood fibres before they can be used with confidence as load-bearing constituents in structural components. The spatial distribution of the hemicelluloses, lignin and cellulose microfibrils, in the layered cell-wall structure, has a strong influence on fibre properties such as stiffness. For instance, the helical structure of the cell-wall layers implies that axial deformation is coupled with torsion.

This coupling is often not accounted for in micromechanical models where generally the fibres are assumed to be transversely isotropic, homogenous and cylindrical, which overlooks the extension-twist interaction and the presence of lumen, e.g. [1]. However, ultrastructural features that govern the fibre properties can be characterised and modelled using micromechanics and composite theory. It would then be possible, at least semi-quantitatively, to assess the influence of ultrastructure (fibril angle, fibril content and distribution) and mesostructure (the layered cell-wall) on the fibre properties that in turn control the engineering properties of e.g. composites, bulk wood and fibre board. For example, it would be possible to determine to what extent the twist-extension coupling affects the stiffness properties of the fibres and ultimately the structural material. In any case, an approach must be based on the recognition that an optimal balance of properties can be achieved by understanding the integration of fundamental properties at multiple scales from the nanoscopic ultrastructural (e.g. cell-wall layer properties) to microscopic (e.g. fibre aspect ratio) to mesoscopic (e.g. fibre orientation distribution) and macroscopic (composite) levels.

Scope and aim

In this work, an analytical method is presented that can be used to study effects of ultrastructural morphology of wood fibres on the effective hygroelastic properties and the stress distribution in the cell wall. A wood fibre is modelled as an assembly of coaxial hollow cylinders made of orthotropic material with chiral structure. The hygroelastic response of the assembly due to axisymmetric loading and moisture content changes is obtained by solving the corresponding boundary value problem. The solution scheme is based on a state space approach by use of a transfer matrix [2–4]. This method is more convenient for treating multilayered systems than conventional methods based on the stress function approach, e.g. Ref. [5]. A specific advantage of the method applied in this paper is that the number of degrees of freedom does not depend on the number of layers. Once the transfer matrix for each layer is found, a global matrix can be assembled by introducing interlayer contact and boundary conditions. The order of the global matrix, used to solve unknown stresses and displacements, does not depend on the number of layers. With the stress function approach, on the other hand, it is necessary to deal with large system of equations to solve undetermined constants in stresses and displacement expression.

The stress function approach been previously employed for modelling elastic properties of wood fibres [6–8]. A novel feature here is the extension to include the hygroexpansion behaviour. Moreover, a simple analytical ultrastructural homogenisation method [9] is used to determine properties of the cell wall layers from properties of the main wood polymers. This method is applicable to multiphase composites, i.e. cell wall material, and is more appropriate to use than micromechanical models for two-phase composites, e.g. Refs. [10, 11], which are frequently applied, e.g. Refs. [6, 7].

The model is employed to investigate the effect of helical structure of wood fibres, i.e. the microfibril angle (MFA), on its hygroelastic properties. The outline of the present paper is as follows. First, a short review of previous modelling work of ultrastructure–property relationships in wood fibres is given. A description of the morphology of wood fibres and the hygroelastic properties of their constituents follows. The modelling procedure is then outlined. Finally the modelling approach is validated, after which results are presented in relation to experimental findings in literature.

Modelling hygroelastic behaviour of wood fibres

Over the years several models of the structure of the fibre have been attempted in order to make mathematical predictions about mechanical properties and behaviour of wood fibres. The discussion on modelling effects of ultrastructure on wood and fibre behaviour here is primarily taken from the review compiled by Neagu [12].

Different scientists have sought to investigate the structure–property relations at different hierarchical levels, e.g. cell wall layer, fibre or wood level, which has resulted in different idealisations of the layered cell wall structure of the fibre. In many cases, the analysis is restricted to two dimensions (2D) by studying a planar element from the wall of a tubular wood cell or a collapsed pulp fibre [13–21]. Fibres were regarded as filament-wound two-phase structure (cellulose reinforcement and hemicelluloses-lignin matrix) and analysed by orthotropic elasticity theory under plane stress conditions by Mark [13]. Page et al. [17] considered only the thickest cell wall layer (i.e. the middle secondary layer S2) and modelled the behaviour of single pulp fibres under tension. The model was used to determine in-plane properties of the cell wall by fitting to experimentally determined stiffness of pulp fibres with the condition of zero shear strain.

The cell wall is often modelled as consisting of the combined layers of neighbouring cell walls in wood, i.e. a double cell wall. These types of models are used to determine the properties of the cell wall in wood under complete shear restraint. This means that absence of external torsional displacements on entire cells is postulated since multiple wall layers of adjacent cells restrain each other from twisting [14]. Mark and Gillis [16] studied the relationship between the longitudinal Young's modulus (E_L) of wood fibres and the MFA in S2 for different sets of

elastic constants of the cellulose. Persson [20] used finite element (FE) method to model a double cell wall consisting of six layers in an antisymmetric lay-up from lumen to lumen. The effect of a change in the MFA of the S2 on the shrinkage or hygroexpansion coefficients was determined. Results showed that longitudinal and transverse hygroexpansion coefficients increase and decrease, respectively, with increasing MFA, while the hygroexpansion coefficient through thickness is almost unaffected.

Well-beaten pulp fibres or pulp fibres of low yield usually collapse, i.e. the square fibre is flattened out so that its inner surfaces come into contact, and have been modelled as an anti-symmetric laminate [18, 19, 21]. This type of laminate models make it possible to account for the coupling between extension and twisting, although usually the twist is set to zero to allow comparison with experiments where the mounting is considered to be firm. Bergander and Salmén [21] showed that properties of hemicellulose are dominating in the transverse direction and MFA of the outer (S1) and the inner secondary cell wall layer (S3) became important especially for high MFA in S2. Also, the higher the relative thickness of S2 the higher is the fibre stiffness at low MFA, and the lower is the fibres stiffness at higher MFA.

A composite tube idealisation of the cell wall has primarily been used to study the behaviour of uncollapsed single fibres under load [6–8, 20, 22–24]. Barber [22] treated the shrinkage of a wood cell represented by a thick-walled circular cylinder as a problem in elasticity. Three dimensional (3D) elasticity theory has been used to analyse the behaviour of wood fibres composed of several concentric anisotropic cylinders mainly for predicting twist of single fibres [6–8, 23]. Lekhnitskii formalism [25] extended to layered cylinders is usually used to solve the problem for axisymmetric loading. The solution scheme is straightforward, i.e. the solution expressions (i.e. stresses and displacements) for each layer are determined first, and satisfaction of the interfacial continuity conditions and boundary conditions is then enforced. Analyses have been extended to include swelling [7] and possibility to prescribe internal pressure [8]. Gillis and Mark [7] predicted axial strain and rotation per unit length in the same order of magnitude as experimental values on never-dried pulp fibres free to rotate at one end under dead-weight loading.

Persson [20] used FE analysis to simulate the deformation behaviour of earlywood fibres idealised as composites tubes with square-like cross section with rounded corners. The analysis revealed that, in addition to the well know deformations due to twist-extension coupling, an in-plane bending moment loading produces an out-of-plane deformation, and conversely, an in-plane shear force loading produces an out-of-plane rotation of the fibres. This behaviour was more pronounced for larger MFA in S2. FE modelling was also used by Gassan et al. [24] to study the influence of a change in cross-sectional shape of a fibre (i.e. from elliptic to circular).

Morphology of wood fibres

Knowledge and understanding of the wood fibre structure is of importance in order to derive or select a suitable micromechanical model. This section focuses on cell-wall ultrastructural models, orientation of the cellulose microfibrils in the different layers and the hygroelastic properties of the main wood polymers, i.e. information significant to simulations of ultrastructural effects. For more detailed information on ultrastructure of wood fibres the reader is referred to Ref. [12].

Ultrastructure

The generally accepted picture is that wood fibres are hollow layered structures with a primary cell wall (cambial wall) on the outside and a secondary cell wall (laid down after the cell has reached its final size and shape) and lumen contained within [26–28]. The different layers shown in Fig. 1a are designated as: the primary wall (P), the outer layer of secondary wall (S1), the middle layer of secondary wall (S2) and the inner layer of secondary wall (S3). In the wood structure the middle lamella (ML) surrounds the wood fibres and holds them together and is therefore not regarded as a cell-wall layer. The primary and secondary walls can be regarded as composites with cellulose being the reinforcing phase in a matrix of hemicellulose and lignin. The distribution of wood polymers across the cell wall is not uniform, and cellulose and hemicellulose content is greater throughout the secondary wall layers than in P [29]. The S1, S2, and S3 are lignified to approximately the same extent.

The ultrastructure of each cell wall layer is often described as being composed by cellulose microfibrils aggregated into larger structures embedded into hemicellulose and enclosed by lignin, as the model proposed by Fengel [30] which Fig. 1b shows. The cellulose microfibrils in a typical softwood fibre are believed to be approximately square with a lateral dimension of 3–4 nm [30], and when aggregated into larger entities, cellulose aggregates have an average dimension of 15–25 nm [31]. Studies have shown that some hemicellulose, particularly the glucomannan type, is closely associated with cellulose aggregates while the lignin matrix is interspaced with xylan entities [32]. The arrangement of the wood polymers on a larger scale is that of a tangential lamellation e.g. Ref. [33]. Adjacent cellulose microfibrils assembled into larger aggregates follow generally similar parallel helical

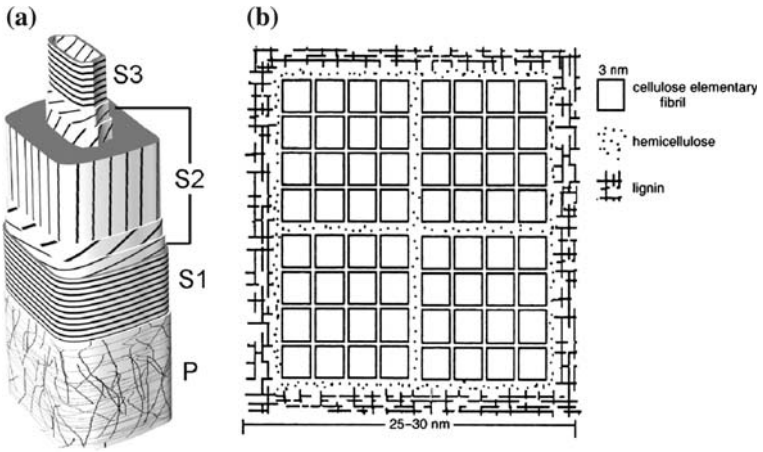

Fig. 1 (**a**) Schematic design of the cell wall of a softwood fibre with different orientation of cellulose microfibrils in the layers [28]. (**b**) Ultrastructural organisation of cellulose microfibrils, hemicellulose and lignin within the wood cell wall [30]

patterns. In the cell wall, they are laid down to form a large number of lamella in concentric adjacent positions to constitute the structural framework of the cell wall.

The angle between the fibre axis and the cellulose microfibrils is known as the MFA, i.e. MFA, and has been shown to define much of the mechanical properties of a wood fibre. The primary cell-wall layer P has microfibrils organised in a loose interwoven texture, considered to be oriented approximately longitudinally and transversely with respect to the tracheid axis in the outer and inner part, respectively. The microfibrils are oriented differently in the S1, S2 and S3, but usually follow an S-Z-S arrangement [34]. A helix is defined as being either S or Z when its direction, as viewed from the outside of the cell, is the same as the centre stroke of the letter. According to the model shown in Fig. 1a, the thin S1 layer is composed of microfibrils oriented approximately perpendicular to the fibre axis. For Norway spruce fibres MFAs varying from 70° to 90° in a single helix have been reported [35]. The central thick S2 layer has cellulose fibrils with a typical Z inclination to the fibre axis. For Norway spruce typical MFA is about 30° for earlywood fibres and about 2°–10° for latewood fibres [36]. The microfibrils in the thinnest layer, i.e. S3, form S-helices with large inclinations to the fibre axis, e.g. for Norway spruce about 40°–50° [37]. It should be mentioned that there is a progressive change in the orientation of the microfibrils through the secondary wall. For instance a gradual shift from an S-helix to a Z-helix from the outer toward the inner part of S1 and from a steep Z-helix to an S-helix from outer toward the inner part of S3, has been reported [37–39]. Furthermore, the orientation of microfibrils within a fibre, in particular in S2, is usually influenced by the presence of pits, i.e. openings that permit passage of fluid [40], which cause local deviation of the MFA. The orientation tends to become flatter between pit openings around which the microfibrils sweep over in a stream-like fashion [38]. It should be kept in mind that pits are an important morphological characteristic of wood fibres. From a structural mechanics point of view these can be seen as natural defects that cause stress concentrations which might result in crack initiation and ultimate structural failure [41].

Some micro- and ultrastructural parameters for softwood fibres are given in Table 1. Typical values of fibre length in wood were found in the review of Brändström [42]. Values of the radial and tangential width, layer thickness are taken from the works of Fengel [43] and Fengel and Stoll [44]. The volume fractions of the wood polymers are given at a moisture content of 12% (i.e. dry condition for wood). They are based on the FE calculations of Persson [20] who accounted for the fact that the wood polymers differ in their moisture absorption properties and computed the change in volume fraction using the ultrastructural model shown in Fig. 1b and initial data given in [43, 45]. It is noted that the volume fractions in P and S1 were assumed to be the same.

Hygroelastic properties of wood polymers

The structural load-bearing component of the cell wall is primarily cellulose which has a high stiffness in the longitudinal polymer chain direction and can be regarded as isotropic with respect to directions in the plane perpendicular the chain direction. Although the mechanical function of the hemicellulose is less evident, it may function as coupling agent between the cellulose and the lignin [46]. Since the hemicellulose molecules tend to be aligned with the cellulose chains it might also be regarded as transversely isotropic. Lignin acts as a bulking or stabilising agent making the cell wall rigid and preventing buckling induced by longitudinal compression [47]. Lignin is usually treated as an isotropic material, although there are indications of a preferred orientation along with the direction of the cellulose aggregates [48]. Published results

Table 1 Structural data for typical earlywood and softwood fibres

		Earlywood (EW)		Latewood (LW)							
Microstructural parameters	Radial width (μm)	39.3		13.1							
	Tangential width (μm)	32.7		32.1							
	Length (μm)	1.28–4.29									
Ultrastructural parameters	Layer	Thickness				MFA			Volume fraction		
									Cellulose	Hemicellulose	Lignin
		(μm)	(%)	(μm)	(%)	(°)	Helix		(%)	(%)	(%)
	S3	0.06	3.0	0.09	2.0	40–50	S		44.3	31.6	24.1
	S2	1.54	78.6	3.84	87.9	0–10 (LW) 30 (EW)	Z		44.3	31.6	24.1
	S1	0.25	12.8	0.34	7.8	70–90	S		18	17.4	64.6
	P	0.11	5.6	0.10	2.3	90 (inner) 0 (outer)	–		18	17.4	64.6
	Total	1.96		4.37							

on the hygroelastic properties of the main wood polymers are very limited, and if not experimentally determined [49–51], existing values are calculated from molecular models [52, 53] or estimated from the behaviour of similar materials [20, 51]. A compilation of different values of engineering elastic constants reported for wood polymers is found in Table 2. Transversely isotropic elastic properties are: the axial and transverse Young's moduli, E_A and E_T, the shear moduli G_A and G_T, and the Poisson's ratios v_A and v_T. The axial and transverse hygroexpansion coefficients are denoted β_A and β_T, respectively.

The elastic properties of cellulose are considered to be independent of moisture changes although it contains small amorphous regions that can absorb water. The hygroexpansion coefficients of cellulose may therefore be neglected. Hemicelluloses though are polar polymers and thus should be softened by polar solvents. Therefore its mechanical properties are strongly affected by changes in moisture content [51]. Elastic parameters for hemicellulose and lignin in Table 2 are given at 12% moisture content which corresponds to a relative humidity condition of 50 and 60%, respectively [50, 51]. The hygroexpansion coefficients of hemicellulose and lignin were calculated based on the assumption of Cave [54] and Persson [20] using an arbitrary ratio of $\beta_T/\beta_A = 2$. The short description of the fibre ultrastructure above as well as the information given Tables 1 and 2 are necessary in attempts to make predictions of hygroelastic properties and behaviour of wood fibres.

Modelling

A wood fibre is considered as long smooth walled composite tube so that secondary effects due to pits, to tapered ends of real tracheids and to ray cells are ignored. Moreover, the MFA is assumed to be constant though the thickness of any one layer of the fibre cell wall. Since wood fibres are hygroscopic and show a complex interaction between the stress–strain behaviour and the moisture content, the discussion on elasticity here is confined to low moisture contents where the fibre is assumed to be linearly elastic with constant elastic parameters. Other simplifying assumptions are that the hygroexpansion is linear and that the moisture content is independent on residual stresses. It should be noted, however, that for large variations in moisture content, local stresses will develop due to the mismatch in hygroexpansion of the constituents. The corresponding changes in free volume can then affect the equilibrium moisture content [55].

The wood fibre is modelled as a circular tube with internal and external radii a and b that can be composed of n anisotropic layers as shown in Fig. 2. The hollow layered

Table 2 Hygroelastic properties of wood polymers

Property	Cellulose	Reference	Hemicellulose	Reference	Lignin	Reference
E_A (GPa)	137	[49]	8	[51]	3.1	[50]
E_T (GPa)	18	[52, 54]	3.4	[54]	3.1	
G_A (GPa)	5.1	[52]	2	[20]	1.2	[50]
ν_A	0.38	[53]	0.3	[54]	0.3	
ν_T	0.48	[54]	0.4	[54]	0.3	
β_L	0	–	0.55	[20, 54]	0.35	[20, 54]
β_T	0	–	1.10	[20, 54]	0.35	[20, 54]

cylinder is subjected to end loads and pressure that do not vary in the z-axis as shown in Fig. 2, hence the stress is independent of z.

The present analysis is limited to cylindrically anisotropic materials. The cell-wall layers can be considered to be orthotropic with the principal directions of the material as shown in Fig. 2. These principal directions are the longitudinal (3-axis), corresponding to the direction of the cellulose microfibrils, and the tangential (2-axis) and radial directions (1-axis). The angle between the longitudinal direction and the plane normal to the z-axis, ϕ (Fig. 2), defines the MFA. The analysis can start by considering the hygroelastic stress–displacement relations for the kth layer referred to the cylindrical coordinates (r, θ, z)

$$\begin{Bmatrix} \sigma_r \\ \sigma_\theta \\ \sigma_z \\ \sigma_{\theta_z} \\ \sigma_{rz} \\ \sigma_{r\theta} \end{Bmatrix}_k = \begin{bmatrix} c_{11} & c_{12} & c_{13} & c_{14} & 0 & 0 \\ c_{12} & c_{22} & c_{23} & c_{24} & 0 & 0 \\ c_{13} & c_{23} & c_{33} & c_{34} & 0 & 0 \\ c_{14} & c_{24} & c_{34} & c_{44} & 0 & 0 \\ 0 & 0 & 0 & 0 & c_{55} & c_{56} \\ 0 & 0 & 0 & 0 & c_{56} & c_{66} \end{bmatrix}_k \begin{Bmatrix} u_{r,r} \\ r^{-1}\left(u_{\theta,\theta} + u_r\right) \\ u_{z,z} \\ u_{\theta,z} + r^{-1}u_{z,\theta} \\ u_{z,r} + u_{r,z} \\ r^{-1}u_{r,\theta} + u_{\theta,r} - r^{-1}u_\theta \end{Bmatrix}_k - \begin{Bmatrix} \beta_1 \\ \beta_2 \\ \beta_3 \\ \beta_4 \\ 0 \\ 0 \end{Bmatrix}_k \Delta C, \tag{1}$$

where σ_r, σ_θ, σ_z, $\sigma_{\theta\,z}$,σ_{rz}, $\sigma_{r\theta}$ are stress components, u_r, u_θ, u_z are the displacements, ΔC is the moisture content change in the material, $(c_{ij})_k$ are the elastic constants and $(\beta_i)_k$ are constants related to the hygroexpansion of the material. The subscript k will be used to denote the kth layer and a comma denotes partial differentiation with the respect to the suffix variable. The 13 elastic constants $(c_{ij})_k$ and four constants $(\beta_i)_k$ in Eq. 1 are components of the matrix in Eq. A9 and the vector in Eq. A10 which are derived from orthotropic layer properties by a rotation about the radial axis as described in Appendix A.

The boundary conditions on the inner and outer surface are $\{\sigma_r \quad \sigma_{r\theta} \quad \sigma_{rz}\}_1 = \{-p_a \quad 0 \quad 0\}$ on $r = a$ and $\{\sigma_r \quad \sigma_{r\theta} \quad \sigma_{rz}\}_n = \{-p_b \quad 0 \quad 0\}$ on $r = b$, where p_a and p_b are internal and external pressure as shown in Fig. 2. The end conditions require that the stress resultants reduce to an axial force, P_z, and a torque, M_t, such that

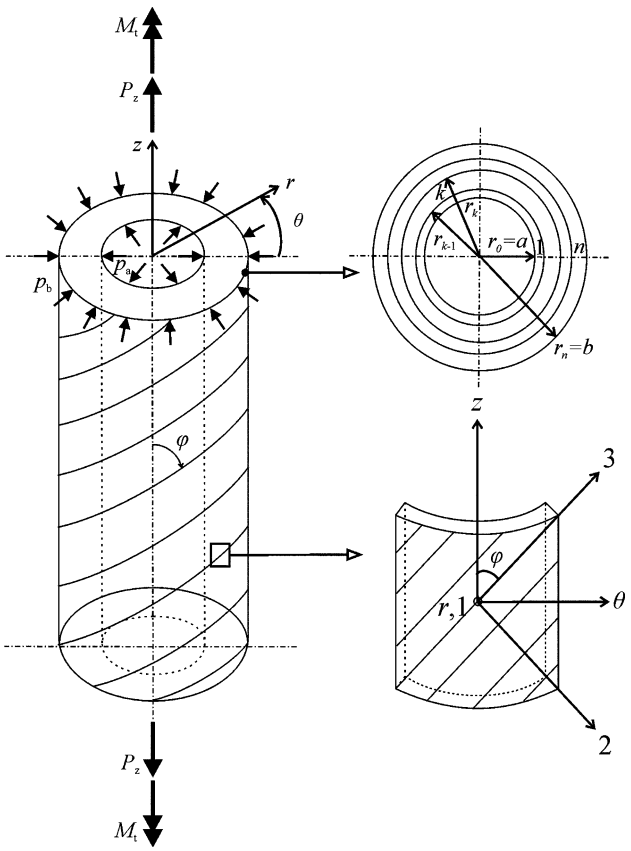

Fig. 2 Schematic drawing of the fibre idealised as an n layered composite cylinder subjected to end loads and internal and external pressures. The relation between principal material axis and the cylindrical coordinate system of the tube is shown

$$P_z = \sum_{k=1}^{n} \int_0^{2\pi} \int_{r_{k-1}}^{k} (r\sigma_z)_k \, \mathrm{d}r \, \mathrm{d}\theta, \tag{2}$$

$$M_t = \sum_{k=1}^{n} \int_0^{2\pi} \int_{r_{k-1}}^{k} (r\sigma_{\theta z})_k r \, \mathrm{d}r \, \mathrm{d}\theta, \tag{3}$$

where r_{k-1} and r_k denote the internal and external radii of the kth layer, thus $r_0 = a$ and $r_n = b$. The condition that the shear resultants vanish at the ends are satisfied when the stress in independent of z [2]. Interfacial continuity conditions at the interface $r = r_k$ between cylinder layer k and $k + 1$ require

$$\begin{Bmatrix} u_r & u_\theta & u_z \\ \sigma_r & \sigma_{r\theta} & \sigma_{rz} \end{Bmatrix}_{k+1} = \begin{Bmatrix} u_r & u_\theta & u_z \\ \sigma_r & \sigma_{r\theta} & \sigma_{rz} \end{Bmatrix}_k, \tag{4}$$

for $k = 1, 2, \ldots, n-1$. The applied loads give rise to an axisymmetric state and produce extension, torsion, radial contraction and circumferential deformation. The expressions for the displacement field and the single equilibrium equation in cylindrical coordinates, that is not identically satisfied for the axisymmetric state, are [25]

$$\{ u_r \quad u_\theta \quad u_z \} = \{ u(r) \quad \vartheta r z \quad \varepsilon z \}, \tag{5}$$

and

$$(r\sigma_r)_{,r} - \sigma_\theta = 0, \tag{6}$$

respectively. The terms associated with rigid body displacement in Eq. 6 have been eliminated and $u(r)$, is an unknown function and the global deformations are axial strain, ε, and rotation per unit length, ϑ.

A state space approach

The state space approach is a useful method for analysis of multilayered structures [2–4, 56, 57]. It is based on casting the equations of elasticity in a mixed form that contains stresses as well as displacements which leads to conversion of the boundary value problem of elasticity to an initial value problem [56]. The state space formalism for thermoelastic analysis of a cylindrically anisotropic body [2, 4] is here used to solve the problem. In this formalism it is important to express the constitutive equations and the field equation, i.e. Eqs. 1 and 6, in a so-called state equation and an output equation in terms of a state vector that consists of unknown variables, analogous to approaches used in control and signal theory. It is noteworthy that $r\sigma_{ij}$ instead of σ_{ij} need to be taken as the stress variables in order to formulate the 3D equations of elasticity in cylindrical coordinates into concise and convenient state and output equations. For the problem at hand, it is natural to take the radial displacement and stress variable, u_r and $r\sigma_r$, as the primary unknown variables because the interfacial continuity condition, Eq. 4, and the boundary conditions are directly associated with them. By taking u_r and $r\sigma_r$ to form the state vector and expressing the stress variables $r\sigma_\theta$, $r\sigma_z$ and $r\sigma_{\theta\ z}$ in terms of them, the state and output equations can be derived using Eqs. 1, 5 and 6. The constitutive equations and the equilibrium equations are first cast into a system of first order differential equations with respect to r to obtain the state equation

$$\begin{aligned} r\frac{\mathrm{d}}{\mathrm{d}r}\begin{Bmatrix} u \\ r\sigma_r \end{Bmatrix}_k &= \begin{bmatrix} -\hat{c}_{12} & c_{11}^{-1} \\ Q_{22} & \hat{c}_{12} \end{bmatrix}_k \begin{Bmatrix} u \\ r\sigma_r \end{Bmatrix}_k + r\varepsilon \begin{Bmatrix} -\hat{c}_{13} \\ Q_{23} \end{Bmatrix}_k \\ &\quad + r\Delta C \begin{Bmatrix} c_{11}^{-1}\beta_1 \\ -\tilde{\beta}_2 \end{Bmatrix}_k + r^2\vartheta \begin{Bmatrix} -\hat{c}_{14} \\ Q_{24} \end{Bmatrix}_k, \\ r_{k-1} &\le r \le r_k \end{aligned} \tag{7}$$

where $\hat{c}_{ij} = c_{ij}/c_{11}$, $Q_{ij} = c_{ij} - c_{1i}c_{1j}/c_{11}$ and $\tilde{\beta}_i = \beta_i - \beta_1 c_{1i}/c_{11}$. The output equation expressed in terms of the primary state variables for layer k, namely u_k and $(r\sigma_r)_k$, then follows as

$$\begin{aligned} \begin{Bmatrix} r\sigma_\theta \\ r\sigma_z\sigma_{\theta_z} \end{Bmatrix}_k &= \begin{Bmatrix} Q_{22} \\ Q_{23} \\ Q_{24} \end{Bmatrix}_k u_k + \begin{Bmatrix} \hat{c}_{12} \\ \hat{c}_{13} \\ \hat{c}_{14} \end{Bmatrix}_k (r\sigma_r)_k \\ &\quad + r\varepsilon \begin{Bmatrix} Q_{23} \\ Q_{33} \\ Q_{34} \end{Bmatrix}_k + r\Delta C \begin{Bmatrix} -\tilde{\beta}_2 \\ -\tilde{\beta}_3 \\ -\tilde{\beta}_4 \end{Bmatrix}_k + r^2\vartheta \begin{Bmatrix} Q_{24} \\ Q_{34} \\ Q_{44} \end{Bmatrix}_k \end{aligned} \tag{8}$$

The judicious arrangement of stress variables results in a system matrix in Eq. 7 independent of r, which makes it possible to solve the state equation with matrix algebra. The state equation plays a key role in the formalism and once it is solved the displacement and stresses follow. Hence, if the radial displacement and radial stress in Eq. 7 are solved the circumferential, axial and shear stress components are obtained from Eq. 8.

Equation 7 is a standard first-order differential equation with a constant coefficient matrix, whose solution is obtained following the work of Tarn and Wang [2] as

$$\{X(r)\}_k = [P(r/r_{k-1})]_k \{X(r_{k-1})\}_k + \{q(r)\}_k, \; r_{k-1} \le r \le r_k \tag{9}$$

where the state vector $\{X(r)\}_k$, the fundamental transfer matrix $\{P(r)\}_k$, and the particular solution associated with the non-homogenous terms in Eq. 7, $\{q(r)\}_k$, are

$$\{X(r)\}_k = \{\, u(r) \quad r\sigma_r(r) \,\}_k^{\mathrm{t}} \tag{10}$$

$$\{P(r)\}_k = [M]_k \begin{bmatrix} (r/r_{k-1})^{(\lambda_1)_k} & 0 \\ 0 & (r/r_{k-1})^{(\lambda_2)_k} \end{bmatrix} [M]_k^{-1} \tag{11}$$

$$\{q(r)\}_k = \left(r_{k-1}[P(r/r_{k-1})]_k - r[I]\right)\left(\{z_\varepsilon\}_k + \{z_{\Delta C}\}_k\right) + \left(r_{k-1}^2[P(r/r_{k-1})]_k - r^2[I]\right)\{z_\vartheta\}_k \tag{12}$$

in which, superscript t indicates matrix transpose, $[I]$ is the identity matrix, $(\lambda_{1,2})_k$ are the distinct eigenvalues of the system matrix in Eq. 7 and the matrix $[M]_k$ consists of the eigenvectors associated with the eigenvalues, i.e.

$$(\lambda_{1,2})_k = \pm(c_{22}/c_{11})_k^{1/2} \tag{13}$$

$$[M]_k = \begin{bmatrix} 1 & -1 \\ (c_{11}c_{22})^{1/2} + c_{12} & (c_{11}c_{22})^{1/2} - c_{12} \end{bmatrix}_k \tag{14}$$

The vectors, $\{z_\varepsilon\}$, $\{z_{\Delta C}\}$ and $\{\, z_\vartheta \,\}$, in Eq. 12 are obtained by solving the non-homogenous part of the state equation as

$$\{z_\varepsilon\}_k = \varepsilon/(c_{11} - c_{22})_k \; \{\, c_{13} - c_{23} \quad c_{13}(c_{12} + c_{22}) - c_{23}(c_{11} + c_{12}) \,\}_k^{\mathrm{t}} \tag{15}$$

$$\{z_{\Delta C}\}_k = \Delta C/(c_{11} - c_{22})_k \; \left\{\, \beta_1(\hat{c}_{12} - 1) + \tilde{\beta}_2 \quad -\beta_1 Q_{22} + \tilde{\beta}_2(c_{11} + c_{12}) \,\right\}_k^{\mathrm{t}} \tag{16}$$

$$\{z_\vartheta\}_k = \vartheta/(4c_{11} - c_{22})_k \; \{\, c_{14}(2 - \hat{c}_{12}) - Q_{24} \quad c_{14}Q_{22} - Q_{24}(2c_{11} + c_{12}) \,\}_k^{\mathrm{t}} \tag{17}$$

Note that Eqs. 15–17 hold only for cylindrically anisotropic materials, i.e. $c_{22} \neq c_{11}$, and if $c_{22} \neq 4c_{11}$. For cylindrically orthotropic, transversely isotropic and isotropic layer material (i.e. $(\lambda_{1,2})_k = \pm 1$) and in the case of layer material with elastic constants $c_{22} = 4c_{11}$, the particular solution, Eq. 12, can be modified according to Refs. [2, 4].

From the interfacial continuity condition in Eq. 4 using the solution for the state vector in Eq. 9 it follows

$$\{X(r_k)\}_{k+1} = [P(r_k/r_{k-1})]_k\{X(r_{k-1})\}_k + \{q(r_k)\}_k \tag{18}$$

for $k = 1,2,\ldots,n-1$. With Eqs. 9 and 18 the state vector containing the unknown radial displacement and stress can be transferred from the inner surface of the cylinder outward, to obtain

$$\{X(r)\}_k = [T(r)]_k\{X(a)\}_1 + \{\Phi(r)\}_k, \quad r_{k-1} \le r \le r_k \tag{19}$$

where the global transfer matrix $[T(r)]_k$ is

$$[T(r)]_k = \begin{cases} [P(r/a)], & k = 1 \\ [P(r/r_{k-1})]_k[T(r_{k-1})]_{k-1}, & k = 2,3,\ldots,n \end{cases} \tag{20}$$

and the vector $\{\Phi(r)\}_k$ transfers the particular solution as

$$\{\Phi(r)\}_k = \begin{cases} \{q(r)\}, k=1 \\ [P(r/r_{k-1})]_k\{\Phi(r_{k-1})\}_{k-1} + \{q(r)\}_k, k=2,3,\ldots,n \end{cases} \tag{21}$$

with $[P(r)]_k$ and $\{q(r)\}_k$ are given by Eqs. 11, 12. The state vector for each layer, i.e. Equation 10, can be connected where the boundary conditions are prescribed by setting $r = b$ in Eq. 19. This allows for the solution of the unknown radial displacement on $r = a$ so that the state vector

$$\{X(a)\}_1 = \left\{T_{21}(b)^{-1}(ap_aT_{22}(b) - bp_b - \Phi_2(b)) - ap_a\right\}^{\mathrm{t}} \tag{22}$$

where $T_{21}(b)$, $T_{22}(b)$ and $\Phi_2(b)$ are components of the matrix and vector given in Eqs. 20–21. The solution for a general problem given in Eqs. 19–22 contains the global deformations ε and ϑ that are related to the end loads through Eqs. 2 and 3 by making use of the output equation, i.e. Eq. 8.

Determining hygroelastic constants of wood fibres

Relations between global deformations and applied loads and change in moisture content must be established since an arbitrary set of ε and ϑ will not yield the stress for a combined action of prescribed loads. It follows that extension, torsion, pressuring and changes in moisture content interact with the applied loads as

$$\begin{Bmatrix} P_z \\ M_t \end{Bmatrix} = \begin{bmatrix} k_{11}\,k_{12} \\ k_{21}\,k_{22} \end{bmatrix} \begin{Bmatrix} \varepsilon \\ \vartheta \end{Bmatrix} + \begin{bmatrix} k_{13}\,k_{14} \\ k_{23}\,k_{24} \end{bmatrix} \begin{Bmatrix} p_a \\ p_b \end{Bmatrix} + \begin{Bmatrix} k_{15} \\ k_{25} \end{Bmatrix} \Delta C \tag{23}$$

where k_{ij} are influence coefficients. These can be found by prescribing the global deformation, internal and external pressure and moisture content change via Eqs. 2, 3, 8 and 19. Prescribing $\varepsilon = 1$ and $\vartheta = p_{\mathrm{a}} = p_{\mathrm{b}} = \Delta C = 0$ in the analysis to determine P_z and M_t from Eqs. 2 and 3 gives $k_{11} = P_z$ and $k_{21} = M_t$ from Eq. 23, and similarly prescribing $\vartheta = 1$ and $\varepsilon = p_{\mathrm{a}} = p_{\mathrm{b}} = \Delta C = 0$, gives $k_{12} = P_z$ and $k_{22} = M_t$, and so on. After obtaining k_{ij} the global deformations due to a combination of applied load and a moisture content change can be determined by a simple inversion from Eq. 23. The radial displacement and stresses in the tube are determined via Eqs. 19–22 and Eq. 8.

The determination of the effective hygroelastic properties of the cylindrical tube, i.e. the wood fibre, is then straightforward. The longitudinal Young's modulus, E_z, and the Poisson's ratio, $v_{z\theta}$, are determined from

$$E_z = \frac{P_z}{\pi(b^2 - a^2)\varepsilon} \tag{24}$$

$$v_{z\theta} = -\frac{u(b)}{b\varepsilon} \tag{25}$$

by solving for ε using Eq. 23 with $p_a = p_b = \Delta C = 0$, given an axial load P_z and $M_t = 0$ in the case the fibre is allowed to rotate freely, or $M_t = P_z(k_{12}/k_{11})$ so that the fibre is prevented from rotating. The radial displacement $u(b)$ is obtained from Eq. 19. Similarly the shear modulus $G_{z\theta}$,

$$G_{z\theta} = \frac{2M_t}{\pi(b^4 - a^4)\vartheta} \tag{26}$$

can be obtained by specifying a torque M_t and $P_z = 0$ if the fibre is free to extend or $P_z = M_t(k_{12}/k_{22})$ to counteract the extension, and solving for ϑ using Eq. 23 with $p_a = p_b = \Delta C = 0$. The effective hygroexpansion coefficients are given by

$$\beta_z = \frac{\varepsilon}{\Delta C} \tag{27}$$

$$\beta_\theta = \frac{u(b)}{b\Delta C} \tag{28}$$

$$\beta_r = \frac{u(b) - u(a)}{(b - a)\Delta C} \tag{29}$$

$$\beta_{z\theta} = \frac{\vartheta b}{\Delta C} \tag{30}$$

where β_z, β_θ, β_r and $\beta_{z\theta}$ denote the longitudinal, circumferential, radial and rotational or shear hygroexpansion coefficients. They are determined by specifying ΔC in Eq. 23 and solving for ε and ϑ which are in turn used in Eq. 19 to obtain the radial displacement $u(r)$.

Tsai-Hill failure criterion

The model presented above can be used for stress analysis and is capable of computing the 3D stress state in the multilayered cylindrical structure. The stresses in cylindrical coordinates for each layer can be obtained from Eqs. 19–22 and Eq. 8 for different loading and boundary conditions. These can in turn be transformed to local material direction using Eq. A5 in Appendix A. Different failure or fracture criteria can then be applied to evaluate the layer stress state and assess failure of the material.

The Tsai-Hill failure criterion, e.g. [58], is here used in an attempt to predict probable locations of failure initiation in flawless wood fibres under tensile loading and different boundary conditions. The 2D criterion is macroscopic and defines an envelope in stress space. If the in-plane stress state lies outside of this envelope, i.e. if the sum of the terms which include the failure strengths of the material is equal to or greater than unity, then failure is predicted. The microscale failure mechanisms could be due to a wide array of processes related to cellulose fibril breakage, hemicellulose-lignin matrix degradation, interfacial failure and all other kinds of interacting failure mechanisms. The criterion takes into account the interaction between different failure modes, i.e. axial, transverse and shear failure. However, the failure mechanism is not specifically identified. The Tsai-Hill criterion is formulated by a failure envelope described by

$$\left(\frac{\sigma_3}{\sigma_{3u}}\right)^2 - \frac{\sigma_3\sigma_2}{\sigma_{3u}^2} + \left(\frac{\sigma_2}{\sigma_{2u}}\right)^2 + \left(\frac{\tau_{32}}{\tau_{32u}}\right)^2 = 1 \tag{31}$$

where σ_3, σ_2, and τ_{32} are stresses in the fibril direction, perpendicular to fibril direction and the in-plane shear stress (Fig. 2), respectively, and σ_{3u}, and σ_{2u} are the ultimate tensile stress in the fibril and transverse direction, respectively, and τ_{32u} is the ultimate shear stress. The radial stress σ_r is neglected in this analysis since it expected to be small for commonly encountered fibre geometries and MFAs [23]. The failure parameters σ_{3u}, σ_{2u} and τ_{32u} can be determined from experimental data on single pulp fibres [59, 60] as outlined in Appendix B. It should be mentioned that there are many theories of failure for anisotropic materials available that consider the 3D stress state which include possibility to predict failure mode, i.e. whether the failure is fibril- or matrix controlled [61]. However, many of these theories include a large number of adjustable parameters (everything from 4 to 15 [61]) that need to be determined from experimental data, which is very limited for wood fibres.

Ultrastructural homogenisation

The hygroelastic properties of each cell wall layer must be given as input to the model. These can be calculated with micromechanical models developed for fibre reinforced composites using the properties of the wood polymers given in Table 2 and the volume fractions in each layer given in Table 1. In order to choose an appropriate model some ultrastructural aspects highlighted previously are recalled. The brief examination of the distribution and spatial arrangement of the main wood polymers revealed

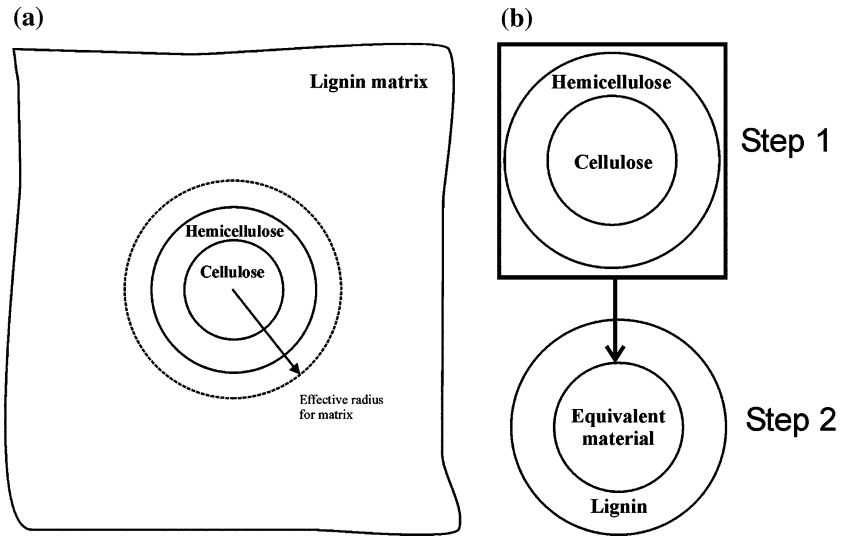

Fig. 3 (**a**) Idealisation of the cell wall layer, i.e. as a two-layered cylindrical inclusion surrounded by an infinite matrix, approximated as a cylindrical jacket around the inclusion (effective radius for the matrix obtained from the phase volume fractions). (**b**) The layer properties are determined in a recursive manner which involves the replacement of inner cylinders, cellulose and hemicellulose phase, with an equivalent homogenous transversely isotropic cylinder (with properties calculated in Step 1) and the subsequent addition of the lignin matrix layer for final calculation (Step 2)

that the cell-wall structure is a multi-phase composite in which cellulose is a discrete and oriented component and the hemicellulose and lignin are blended together to form a surrounding matrix. Due to lack of experimental data it is not possible to differentiate hemicellulose associated with cellulose or with lignin (glucomannan and xylan, respectively), regarding their mechanical function and properties within the cell wall as can be done morphologically [32]. With reference to Fig. 1b, the each cell wall layer is treated here as three-phase composite built up by continuous cellulose microfibrils finely dispersed into a hemicellulose phase that is embedded in a lignin matrix.

To estimate or bound the overall elastic moduli of fibre reinforced materials, the auxiliary problem of a one or two-phase cylinder embedded in an unbounded matrix of another material (e.g. Fig. 3a), subjected to uniform conditions at infinity has been used extensively [62–65]. The Composite Cylinder Assemblage (CCA) model developed by Hashin and Rosen [62] for isotropic constituents, and generalised to anisotropic constituents by Hashin [63], gives exact solutions for four of five effective elastic moduli of a unidirectional layer: the transverse bulk modulus k, the longitudinal Young's modulus E_L, the Poisson's ratio ν_{LT}, and the longitudinal shear modulus G_{LT}. The transverse shear modulus G_T is not determined exactly with the CCA model, but close bounds can be established. The limitation is related to the used homogenised boundary conditions, in displacements or in tractions, which do not exactly correspond to the conditions on cylindrical boundary in a homogenised material. This problem was solved by Christensen and Lo [64] with a generalised self-consistent scheme, i.e. considering an infinite effective composite with unknown G_T and an embedded cylindrical subdomain consisting of an equivalent fibre-matrix microstructure. These models were developed for two-phase composites and cannot be used directly for the tree-phase cell-wall layer composite considered here. However, an extension to N-phase composites has been made. Sutcu [9] proposed a simple algorithm to calculate effective elastic constants and thermal expansion coefficients for a uniaxially aligned composite made of an arbitrary number of coatings on transversely isotropic fibres. The model considers only two concentric cylinders at a time and uses CCA expressions for k, E_L, G_{LT}, ν_{LT} and the thermal expansion coefficients [63, 66], and Christensen and Lo's [64] estimate for G_T in a recursive manner. Generalisation of the Hashin's CCA model and Christensen and Lo's generalised self-consistent approach to the case of composites made of heterogeneous multilayered has been made by Hervé and Zaoui [65] and Marklund [67] for transversely isotropic and orthotropic constituents, respectively.

The micromechanical approach selected here to determine the properties each cell-wall layer follows the work of Sutcu [9]. Each cell wall layer is considered as a concentric cylinder composed of an inner cellulose core, an adjacent hemicellulose cylinder surrounded by a third cylinder composed of lignin as shown in Fig. 3a. The procedure to compute the hygroelastic properties of each cell wall layer is schematically depicted in Fig. 3b. First the properties of the innermost two cylinders are calculated, i.e. the cellulose

and hemicellulose cylinders. The properties k, E_L, G_{LT}, ν_{LT} and the longitudinal and transverse hygroexpansion coefficient, β_L and β_T, (assuming analogy with thermal expansion) are given by the CCA model [63, 66], while G_T is obtained with Christensen and Lo's formula [64] modified for transversely isotropic properties as in Ref. [9]. The transverse Young's moduls and Poisson's ratio, E_T and ν_T, follow from the well-know relations $E_T = 2(1 + \nu_T)G_T$ and $k = 1/(4/E_T - 1/G_T - 2\nu_A^2/E_A)$. The final formulae can be found in Ref. [9]. In a second step, the procedures above are repeated where the cellulose and hemicellulose cylinders are replaced with an equivalent homogenous transversely isotropic cylinder in a lignin matrix. The same formulae are then used to calculate the final properties of the cell wall layer. It should be mentioned that k, E_L, G_{LT}, ν_{LT}, β_L and β_T can be derived exactly by using the recursive algorithm, which coincides with the CCA model for a two-phase composite as shown by Hervé and Zaoui [65]. In order to determine the transverse shear modulus a condition of self-consistency condition has to be imposed [65], where the recursive algorithm [9] for transverse properties is used only approximately. However, Hervé and Zaoui [65] compared the two approaches and the error made by using the recursive algorithm was very small: less than 1% for idealised fibre structure considered by Sutcu [9].

Results and discussion

In this section, the modelling approach will be first validated with FE element calculations and other more conventional analytical methods from literature. Thereafter, simulations on an idealised thick-walled cylindrical fibre are performed to give some examples of applicability of the method. Predicted hygroelastic properties are compared with experimental findings for softwood fibres from literature. Stress analysis is carried out for qualitative prediction of location of failure initiation and to investigate trends that might be linked to experimental observation of fracture in real fibres. All numerical results are computed with MATLAB, where the displacements and stresses through the thickness as well as the influence coefficients in Eq. 23 follow the solution procedure given above.

Validation

The elasticity problem of a cylindrically anisotropic circular tube subjected to axisymmetric loading has been studied extensively in the literature, both analytically and numerically. Examples of applications differ widely e.g. prediction of twist in wood fibres [6, 7, 23], stress analysis of flax fibres [8], investigation of mechanical properties of multilayered filament-wound pipes under internal pressure [68, 69], prediction of the effective thermoelastic behaviour of helical carbon nanotube arrays [70, 71]. The same six model fibres analysed by Tang [6] are modelled with the state space approach and results are evaluated in comparison to the FE solution of Barrett and Schniewind [23]. Table 3 gives the predicted values of axial force and twist due to applied unit axial strain in comparison to FE results of Barrett and Schniewind [23]. There is excellent agreement between FE results and those of the analytical analysis employed here, as can be seen in Table 3.

The results of Tang [6], who used an analytical model based on Lekhnitskii stress function approach [25], are not shown since they are inconsistent with regard to shear deformation in the tangential-axial plane. Tang [6] included $\sigma_{\theta z}$ in the interfacial continuity condition, e.g. Equation 4, which implies that layers are free to twist with respect to each other, which is not the case in a real fibre where the various layers will have to twist as a unit. The same questionable approach was used by Davies and Bruce [8]. Therefore, a stress function approach extended to

Table 3 Predicted values of axial force and twist under unit axial strain applied to the idealised fibre models of Tang [6] in comparison with finite element analysis (FEA) results of Barrett and Schniewind [23]

Model fibre [6]	Free rotation						No rotation		
	P (10^{-5}N)		Δ (%)	ϑ (degrees/cm)		Δ (%)	P (10^{-5}N)		Δ (%)
	State space approach	FEA [23]		State space approach	FEA [23]		State space approach	FEA [23]	
I-1	0.4971	0.4965	0.12	46.11	46.14	–0.07	0.7631	0.7631	0.00
I-2	1.0681	1.0640	0.38	67.85	68.48	–0.93	3.2303	3.3756	–4.50
I-3	0.7509	0.7507	0.03	65.52	65.49	0.04	1.7395	1.7395	0.00
II-1	0.6500	0.6486	0.22	110.35	110.42	–0.06	1.6892	1.6892	0.00
II-2	1.6191	1.6280	–0.55	135.86	136.53	–0.49	8.5235	8.6656	–1.67
II-3	1.4683	1.4683	0.00	115.92	115.87	0.04	3.9580	3.9580	0.00

The symbol Δ denotes relative difference between the predictions in this paper and the FEA results

layered cylinders by Jolicoeur and Cardou [5] was used instead to solve the problem for axisymmetric loading and compared to the state space approach results.

The results obtained with the model of Jolicoeur and Cardou [5] were found to be equivalent to those of the present model. The solution scheme of the stress function approach is straightforward. For each layer there is a stress and displacement function with a number of unknown constants. Satisfaction of the interfacial continuity and boundary conditions, will result in a non-symmetric matrix of order $(4n+2)\times(4n+2)$ for the solution of undetermined constants in stresses and displacement equations. Hence, due to the layerwise treatment it is necessary to deal with large system of equations. This makes the stress function approach ineffective in treating a multilayered system in which interfacial continuity conditions require displacement as well was traction to be continuous. However, with the state space approach, which expresses stresses and displacements in a state equation, i.e. Eq. 7, in which the unknown is the state vector, Eq. 10, the interfacial continuity and boundary conditions are taken into account in a simple manner. Once the transfer matrix for each layer is found, Eq. 11, a global matrix, Eq. 20, can be assembled by introducing interlayer continuity, Eq. 4, and boundary conditions. The order of the global matrix does not depend on the number of layers, which is a unique feature of the state space approach analysis. Moreover, the solution requires only matrix operations and eigensolutions of 2×2 matrices for the axisymmetric state considered here.

Simulation

The analytical method is here employed to predict the hygroelastic properties of the latewood fibre type with properties given in Table 1. The fibre is modelled as consisting of three layers, i.e. S1, S2 and S3. The influence of P is neglected since it contains less cellulose and has microfibrils organised in a loose structure in contrast to the secondary layer. Besides, it is likely that it will be removed during most fibre extraction processes (see e.g. Ref. [41]). The cross-sectional area of the cell wall and lumen are obtained from the radial and tangential width and the cell wall thickness given in Table 1, assuming a rectangular-box shaped cross-section. These are converted to a cylinder of equivalent area, with a cross-sectional area fraction of the lumen $(a/b)^2 = 0.24$, which is used together with the thickness fraction of each layer to calculate the radii of the various layers. The MFA in S1 and S3 was chosen to 80° and 50° in an S-helix, respectively. The MFA in S2 is varied from 0° to 50° to cover commonly reported fibril angles for softwood fibres [12].

The hygroelastic properties of each cell-wall layer are calculated with the micromechanical approach described previously using the elastic properties of the wood polymers given in Table 2 and the volume fractions in each layer given in Table 1. Transversely isotropic elastic constants and hygroexpansion coefficients for S1, S2 and S3 used as input to the modelling are given in Table 4.

It is worth mentioning that this approach has been compared in another work, Ref. [72], with the results of Persson [20] who used a homogenisation procedure and FE method on the ultrastructural model of Fengel [30] shown in Fig. 1b. The results of the analytical micromechanical approach compared well with those of Ref. [20] for the longitudinal and transverse Young's modulus. The difference between the predicted shear moduli was slightly larger, which could be attributed to the fact that ultrastructural model of Fengel [30] is not isotropic in the 1–2 plane.

The elastic properties are predicted for two different conditions:

- free rotation ($M_t = 0$), i.e. the fibre is allowed to rotate and the resultant torsional moment equals to zero, and
- no rotation $(\vartheta = 0)$, i.e. the fibre is rotationally constrained, corresponding to zero twist. For prediction of $G_{z\theta}$ this condition corresponds to no axial extension, i.e. $\varepsilon = 0$.

These represent extreme case of elastic response with the latter is closest to behaviour in either wood, composites or paper where fibres are surrounded by other fibres, embedded in a polymer matrix or constrained between fibre–fibre bonds, respectively.

Elastic properties

The predicted E_z, $v_{z\theta}$ and $G_{z\theta}$, i.e. Eqs. 24–26, are shown in Fig. 4a–c. The dotted line represents the response of a fibre that is allowed to rotate freely (i.e. $M_t = 0$), while the continuous line is the response of a fibre that is constrained (i.e. $\vartheta = 0$ for E_z, $v_{z\theta}$, and $\varepsilon = 0$ for $G_{z\theta}$). It may be seen from Fig. 4a that E_z is extremely sensitive to the helical angle of the cellulose microfibrils in S2, which has also

Table 4 Hygroelastic properties of the cell wall layers calculated with the recursive algorithm of Sutcu [9] and volume fractions and properties of wood polymers given in Tables 1 and 2, respectively

	$E_{11} = E_{22}$(GPa)	E_{33}(GPa)	$G_{23} = G_{13}$ (GPa)	G_{12}(GPa)	$v_{23} = v_{13}$	v_{12}	$\beta_{11} = \beta_{22}$	β_{33}
S3/S2	6.08	64.0	2.54	2.14	0.03	0.42	0.44	0.02
S1	4.20	28.1	1.64	1.49	0.05	0.41	0.47	0.05

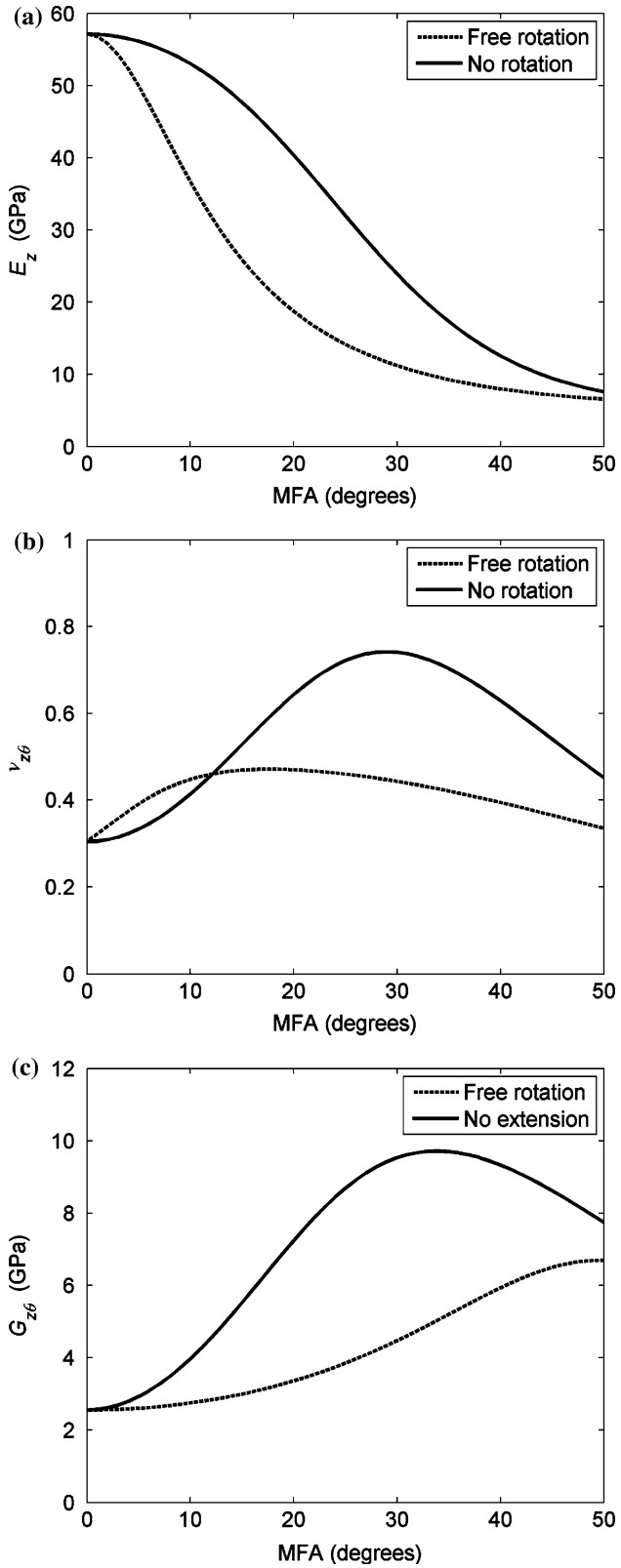

Fig. 4 Predictions of elastic parameters: (**a**) E_z, (**b**) $\nu_{z\theta}$ and (**c**) $G_{z\theta}$ as function of the MFA showing the effect of the twist-extension coupling on the behaviour of (-) constrained fibres and (–) fibres that are allowed to twist

been demonstrated previously by Page et al. [17] in their extensive measurement of the axial modulus of single wood pulp fibres. The predictions of E_z here fall well within the range from 7 to 52 GPa reported for various latewood pulp fibres with different MFA in S2 [73–79]. It should be mentioned that structural changes and damage of the internal fibre structure during any pulping process will result in an effective stiffness reduction and the common observed tendency is that mechanically defibrated, fully bleached or low lignin content fibres generally have lower stiffness than chemically defibrated fibres with higher lignin content [1, 80]. Predictions with the analytical model in this work have also been compared with FE simulations on a wood fibre with the ''real'' geometry characterised by microscopy of microtomed cross sections. It was shown that the analytical model slightly overestimates E_z for both zero torque and zero twist cases, with the maximum deviation being 12% for the latter case for a range of MFA from 0° to 30° [12].

Figure 4a shows as expected that fibres not allowed twisting exhibit a stiffer response. Also for fibres that are allowed to twist freely, of the value of E_z drops earlier with increasing MFA. The results clearly indicate that the twist-extension coupling has significant effect on the elastic behaviour of fibres that are allowed to rotate freely as compared with rotationally constrained fibres. Figrue 4b, c show that $\nu_{z\theta}$ and $G_{z\theta}$ exhibit similar sensitivity to twist-extension coupling. Both are a strong function of the MFA with maximum values corresponding to the constrained case. The Poisson's ratio shows only modest response to changes in MFA for the case of free rotation, but significant dependence if rotation is not allowed. The shear modulus is a monotonically increasing function of the MFA as has also been shown by Persson [20]. However, if the fibre is not allowed to extend while rotating, $G_{z\theta}$ exhibits significant dependence upon MFA, achieving maximum of almost 10 GPa at MFAs around 30°. The predicted shear modulus for a typical latewood fibre, i.e. MFA 0–10° (Table 1), shows little variation and is within the experimentally determined range of 1.2 to 3.5 GPa for latewood kraft fibres [81, 82].

Hygroexpansion coefficients

The predicted effective hygroexpansion coefficients β_z, β_θ, β_r and $\beta_{z\theta}$ are shown in Fig. 5. The form of the curves for β_z, β_θ and β_r are in good general agreement with that of the ones of Persson [20] based on a FE modelling of a double cell wall. The through-thickness hygroexpansion is as expected almost unaffected by changes in MFA, and the value of slightly under 0.5 strain per relative change in moisture content is close to experimental data of [83] who

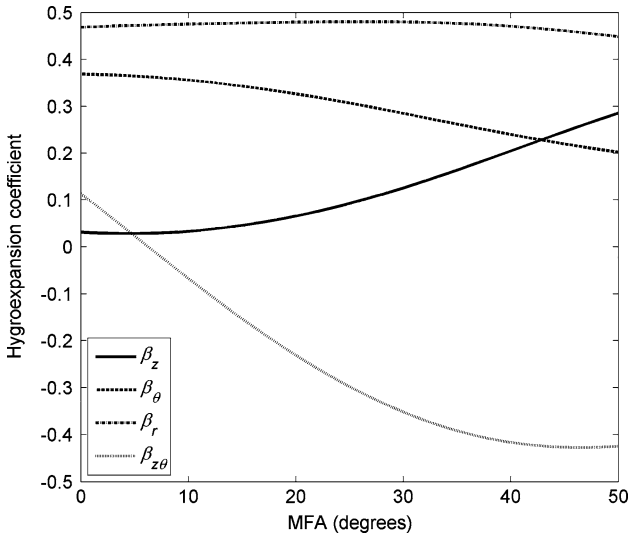

Fig. 5 Predicted effective hygroexpansion coefficients

measured 20% shrinkage of the fibre wall from fibre saturation at about 30% of moisture content to dry conditions. Persson [20] calculated somewhat higher values of 0.61–0.67 for different properties of the wood polymers and fibril angles, assuming that hemicellulose does not expand in the longitudinal direction. Hence the discrepancy is attributable to factors that are different in the two models, such as the hygroelastic properties of the wood polymers, the relative portion of the layers in the cell wall, etc.

The expansion in the longitudinal direction is small compared with that of the transverse and circumferential directions for low MFAs. Comparing predicted β_z for free hygroexpansion of a model fibre, with experimental data on tiny wood blocks ($2 \times 2 \times 25$ mm) of Radiata pine [84] indicates that the theoretical model provides solutions of correct functional form and order of magnitude. Twisting behaviour of single fibres may be expected to be reflected at higher geometrical scales for structures of non-massive cross-section (e.g. small wood blocks or paper), albeit to a smaller degree as shown by Schulgasser and Witztum [85].

Figure 5 also shows that β_z increases and β_θ decreases with increasing MFA which is in accordance with experimental behaviour. This is also expected since the hygroexpansion strains and elastic properties are inversely related. It was shown by Schulgasser [86] that a linear relation exists between the macroscopic strain in an unrestricted composite in a certain direction due to a uniform change in moisture content and the strain in that direction due to a unit uniform pressure applied to the composite. This relationship writes

$$\beta_{\mathrm{d}} = m_1 S_{\mathrm{d}} + m_2 \tag{32}$$

where β_{d} is the hygroexpansion coefficient of the macromaterial in a direction 'd'. The parameters m_1 and m_2 are material constants dependent on hygroelastic properties of the constituents as defined in Ref. [86]. The strain in that direction 'd' due to a unit uniform pressure is

$$S_{\mathrm{d}} = \frac{1}{E_{\mathrm{d}}}(1 - v_{\mathrm{de}} - v_{\mathrm{df}}) \tag{33}$$

where 'e' and 'f' denote the two other principal directions, and the meaning of E_{d}, v_{de}, v_{df} is self-evident. Further, Schulgasser [86] considered experimental data on materials such as wood, particle board and paper, and showed that for a material constituted at a microscopic scale of the fibre cell wall, the expansion caused by a moisture content change is determined by the microstructure of the material predominantly through the elastic compliance of the material in that direction, i.e. the aforementioned linear relationship. It was mentioned that although the compliance dominates the relation, the influence of Poisson's ratios need not necessarily be negligible. This findings suggest that no reduction or increase of the expansion in a given direction can be achieved through varying the microstructure without concomitantly reducing or increasing the compliance in the direction of interest in the same proportion. The same argument holds when the ultrastructure of the cell wall material is considered. From a physical point of view, this can be interpreted as high stiffness is assured by a high density of covalent bonds in a cross section of an oriented polymer, and a high swelling capacity is concurrently assured by a high density of hydrogen bonds transverse to the polymer backbone. Figure 6a shows that when the ultrastructure is altered by a change in MFA of S2, a reduction in E_z, i.e. increase of the compliance in the longitudinal direction, is accompanied by an increase in β_z.

In Fig. 6b, β_z is plotted versus $(1 - v_{z\theta})/E_z$, which is the relation in Eq. 33, without the Poisson's ratio v_{zr} which had to be neglected since it could not be calculated with the analytical model. Figure 6b indicates that the linear relation between hygroexpansion and elastic compliance in the longitudinal direction is valid for MFAs above 10°. A linear regression is made excluding the data points corresponding to MFAs below 10°, and the corresponding fit is shown in Fig. 6b. The immediate implication of this relation is that knowledge of the hygroelastic behaviour of the cell wall material together with knowledge of the elastic behaviour of the fibre (i.e. compliance and Poisson's ratios) is sufficient to determine the hygroexpansion behaviour of the fibre. Conversely, knowledge of the elastic and the hygroexpansion behaviour of the wood fibre may be used to determine the hygroelastic behaviour of the cell wall in the principal material directions from the slope and the intercept of the fit in Fig. 6b, i.e. m_1 and m_2 in Eq. 32. The linear relation shown in Fig. 6b emphasises that the

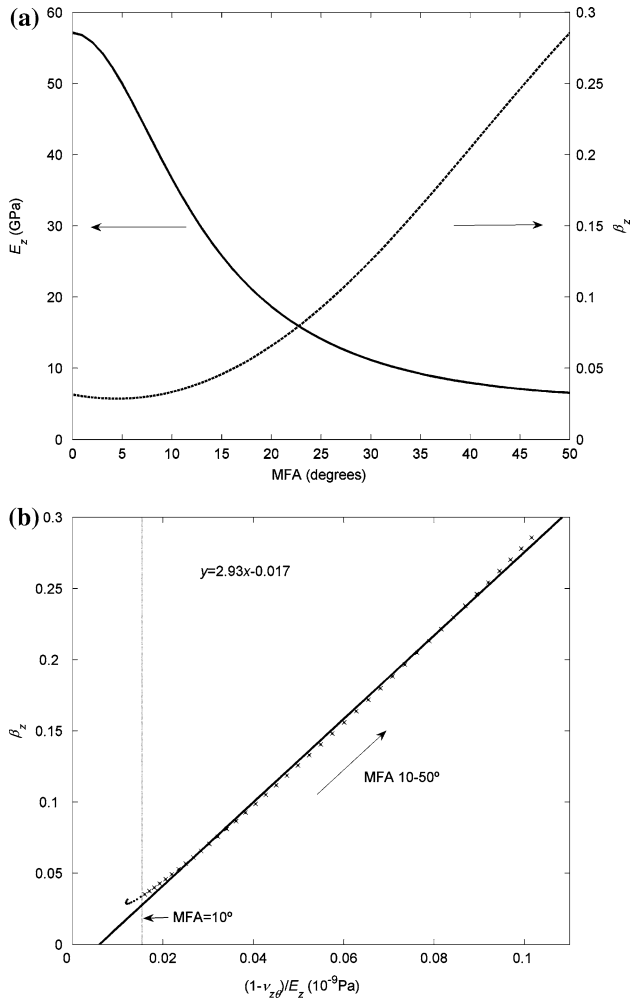

Fig. 6 (**a**) Reduction in E_z and concomitant increase in β_z as the MFA in S2 is increased. (**b**) Relation between β_z and the compliance $1/E_z$, corrected with the Poisson's ratio, for MFAs from 0° to 50°. The linear regression and the corresponding equation apply to data points above a MFA of 10°

ultrastructure will influence the expansion behaviour of the cell wall in the same way as it influences its compliance behaviour.

Results for the effective shearing hygroexpansion $\beta_{z\theta}$ in Fig. 5 reveals a relatively large value compared with the effective longitudinal property and indicates twisting is the dominating deformation mechanism when fibres are subjected to changes in moisture content. This is in accordance with experiments [7] as well as FE calculation [20] on single wood fibres. The experimental work of Gillis and Mark [7] showed that on wetting, the upper end of a fibre (with *Z*-helix in S2 as schematically depicted in Fig. 2) will rotate counterclockwise with respect to the bottom end and on drying the direction is reversed. This is what the theoretical curve in Fig. 5 shows. However, there is a small transition angle for which there will be no twist of the fibre due to the counter-balancing effect of the S1 and S2 layers. Gillis and Mark [7] measured that individual pulp fibres of Virginia pine twist on average up to five full turns, from wet to dry conditions, and since the average length was 2.5 mm the twist might reach 720°/mm. The analytical method here predicts a twist of about 640°/mm for a change in moisture content from 30% to 0%, at the MFA of maximum twist 45°. Persson [20] used theory for large-deformation including an orthotropic elastoplastic material formulation and FE method and calculated a twist 360 °/mm for a change of moisture content from saturated to dry conditions. It should be pointed out that the validity of the small strain analysis when applied to cases of large changes of moisture content is questionable and needs further study. Furthermore, better knowledge of influence of time, temperature and moisture content on the elastic properties of the wood polymers is needed. The elastic constants used in this paper might be useful for calculation of deformation taking place in the 0–12% moisture content range since changes in elastic constants are relatively small near oven dry conditions [51].

Stress analysis

The model also allows for prediction of the stress distribution in the cell wall of idealised cylindrical wood fibres. Figure 7a, b show the relative stresses that develop in the cell wall of a fibre, with MFA of 30 ° in S2, subjected to uniaxial tension for the two different boundary conditions considered here. The relative stresses in a fibre that is allowed to twist freely shown in Fig. 7a can be compared with the case when the fibre is rotationally constrained shown in Fig. 7b. It can be seen that introduction of the no rotation constraint tends to reduce the radial variation of stress and the maximum value of normal stress, σ_z, particularly in the S2 layer. This tendency is accordance with FE results [23] and suggests that an improved mechanical efficiency may be obtained when the fibre is restrained. The predicted relative radial stresses for varying MFA in S2 are always an order of magnitude lower than the other stress components. Small tensile radial stresses (maximum of about 5% of the applied stress) occur at S1-S2 and S2-S3 interface when fibre is free to twist. For the no twist case, compressive radial stresses develop, which suggest an increase in load transfer between cell wall layers. In this case, positive stresses occur only at the S2-S1 interface for high MFA at around 30 ° (Fig. 7b) and above.

The global stresses in the fibre cell wall (Fig. 7a, b) can be transformed to local material direction, using Eq. A5, and the Tsai-Hill failure criterion, Eq. 31, can then be applied to predict probable locations of failure initiation. The failure parameters σ_{3u}, σ_{2u} and τ_{32u} that enter the

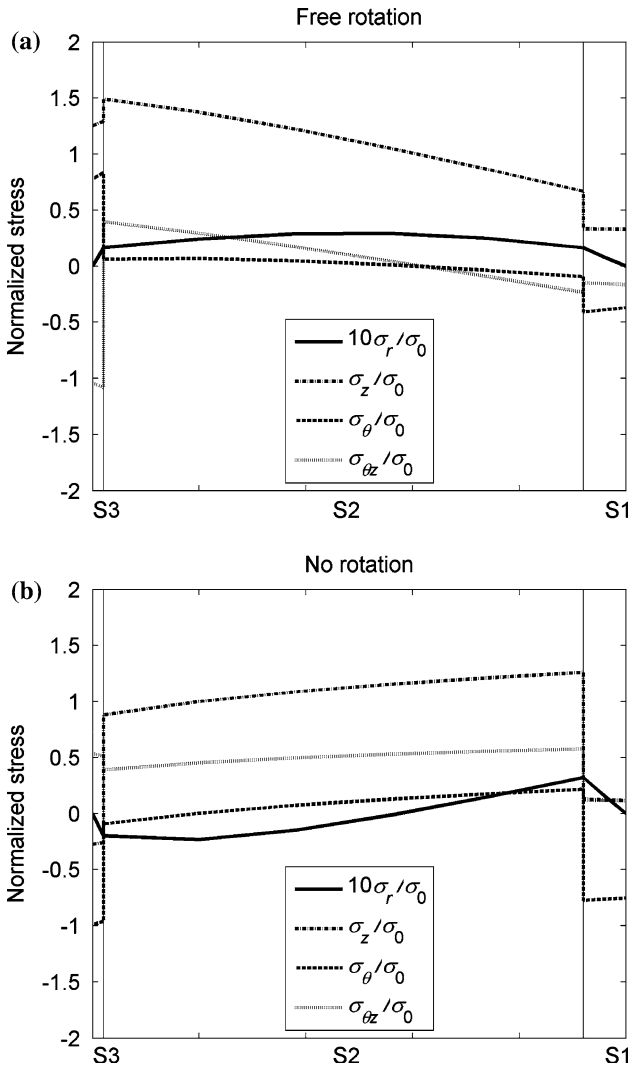

Fig. 7 Normalised stress distribution in a fibre model (**a**) without and (**b**) with constraint on rotation, and for a MFA of 30° in S2. The stress due to applied tensile loading is denoted σ_0

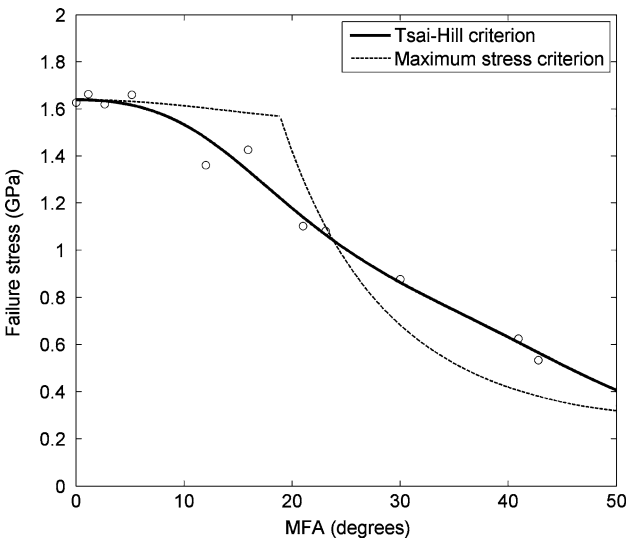

Fig. 8 Tsai-Hill failure and the maximum strength criterion fitted to the experimental data of El-Hosseiny and Page [59]

failure function of Tsai-Hill were determined using the experimental data of El-Hosseiny and Page [59] as outlined in Appendix B. El-Hosseiny and Page [59] determined the tensile strength of kraft pulp fibres with different MFA in S2. The equations in Appendix B contain also relative elastic constants and the Poisson's ratio of the fibres. Values of $E_3/E_2 = 10.3$, $E_3/G_{32} = 0.08$ and $\nu_{32} = 0.32$ were derived from the variation in fibre Young's modulus with MFA of the same sample fibres by El-Hosseiny and Page [59] using the method given in Ref. [17]. Figure 8 shows the upper bound of experimental data of El-Hosseiny and Page [59] together with the corresponding fit to Tsai-Hill failure function. It should be mentioned that there is a great variability in the strength (as well as stiffness) of wood fibres due to damage and natural imperfections, and the upper bound can be interpreted as the strength of those fibres without observable defects [59]. The failure parameters were determined to, $\sigma_{3u} = 1.64$ GPa, $\sigma_{2u} = 144$ MPa and $\tau_{32u} = 291$ MPa. Hence the strength in the direction of the microfibrils is about 6–12 times the strength of the material in shear or in transverse direction, showing the significant anisotropy of the fibre wall material. In Fig. 8, a fit to the maximum stress criterion is shown which was made using the stresses given in Eqs. B1–B3. It is clear this criterion is not suitable to predict a tensile strength of wood fibres for these experimental data.

The stresses arising from a given loading and boundary condition can now be used to predict Tsai-Hill failure function, i.e. the left-hand side of Eq. 31. Only stresses in S2 are of interest since failure of the thin S3 and S1 are expected to have little influence on the overall strength of wood fibres. The radial stress, i.e. σ_r, is neglected since it has been shown to be very small in comparison to other stress components (Fig. 7a, b). Local stresses in S2 were computed for the two boundary conditions as function of the MFA in S2 under an arbitrary chosen applied axial stress of 0.3 GPa. A closer examination of the local stresses trough the thickness of the S2 layer revealed that stresses reach maximum values either at the interface between S1 and S2 or at the interface between S2 and S3 for MFAs from 0° to 30°, depending on the boundary conditions. At higher angles the position of maximum stress within S2 may vary, however in computation of the Tsai-Hill failure function only the stress state in at the S1-S2 and S2-S3 boundaries are considered. Results are presented in Fig. 9a, b for a change in MFA in S2 from 0° to 50°. Figure 9a shows the predictions of the Tsai-Hill failure function in case the fibre is allowed to rotate under applied

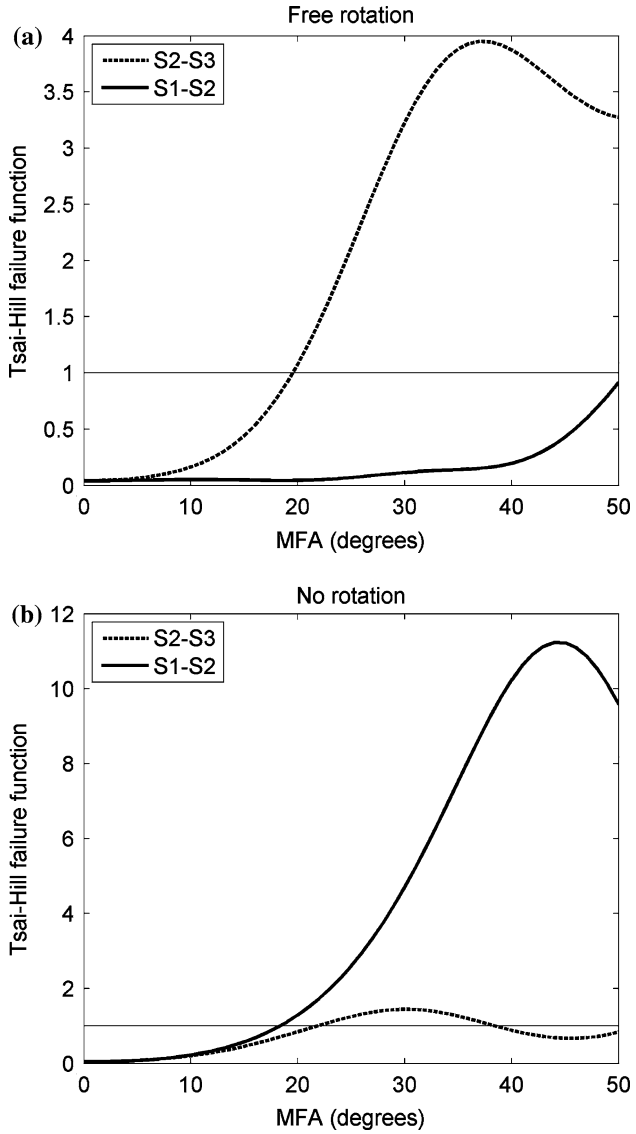

Fig. 9 Tsai-Hill failure function predicted for a fibre subjected to a tensile stress in case the fibre (**a**) is allowed to rotate, and (**b**) not allowed to rotate. Only stress state at the S1-S2 and S2-S3 interfaces are considered, where maximum stresses are expected for MFAs under 30°

tensile stress. In Fig. 9b, the equivalent is plotted for a rotationally constrained fibre under applied tensile stress.

Results show in the rotationally constrained case, that probable location of failure may be expected in the region of S2 close to S1 (Fig. 9b), while for a fibre segment free to twist regions in S2 close to S3 (Fig. 9a). The general experimental evidence that exists for wood fibres is that failure initiates in S1 or at the S1-S2 boundary [13]. FE calculations on fibre segments with irregular shape characterised with microscopy showed similar indications [87]. For constrained fibre segments failure initiation may be expected at the S1-S2 interface, while for free fibre segments it may be expected in the vicinity of the S2-S3 interface. The failure mechanism cannot be specifically identified with the Tsai-Hill criterion, which however takes in account the interaction between different failure modes, i.e. axial, transverse and shear failure. Nevertheless, inspection of the relative magnitudes of the terms in Eq. 31 gives an indication of the likely contribution of the three modes. A quick check of the relative contribution of the terms in Eq. 31 related to each failure parameter showed that axial failure controlled by the strength of the cellulose microfibrils can with certainty only be expected for MFAs very close to zero. Considerable interaction takes place for higher MFAs up to about 30°, where the transverse tensile component will dominate and hence the most likely failure mechanism will be transverse rupture of the hemicellulose-lignin matrix. Hence, it is difficult to point out a specific failure mechanism on the region for MFAs usually encountered in wood fibres, e.g. 0–30°, the exception being when microfibrils are exactly aligned with the fibre axis as mentioned previously.

Stress analysis of cylindrical models of wood fibres can be useful to indicate qualitative failure trends and if combined a 3D failure criteria (e.g. Ref. [61]) perhaps even failure mechanism. In the future, however, it is necessary that this analysis is complemented with experiments on single fibres as well as calculations on fibres with the irregular geometry characterised as in Ref. [87] to obtain quantitative data. In any case, it should always be kept in mind that natural defects such as pits, dislocations and voids are likely to act as stress concentrators, and serve as location of failure in reality e.g. Ref. [41].

Conclusions

A wood fibre has been modelled as an assembly of coaxial hollow cylinders made of orthotropic material. The state space approach in combination with the transfer matrix [2, 4] has been used to solve a 3D elasticity theory problem. A micromechanics based approach [9] was applied at the ultrastructural level to obtain the properties of the cell wall layers from properties of the wood polymers. The analytical modelling approach allows for accurate assessment of the stresses in thick-walled cylinder models of wood fibres. The approach can be useful to investigate ultrastructure–property relations in wood fibres. Specifically, hygroelastic properties can be predicted and stress analysis can be performed to provide qualitative failure trends.

The model has been validated with FE calculations [23] and an analytical model based on the stress function approach [5]. The numerical results presented in this paper are equivalent with the numerical solution based on the more conventional stress function approach [5]. An advantage of the presented method is that the number of degrees of freedom is independent of the number of layers

in the composite tube. Mechanical strain was extended to also include hygroexpansion. Moreover, the model can accommodate an arbitrary number of layers to study effects of a progressive change in MFAs on hygroelastic behaviour of wood fibres.

The applicability of the method has been demonstrated with simulations on a characteristic softwood fibre with properties taken from literature. The model was shown to capture experimentally determined hygroelastic behaviour of wood fibres. The results indicate that the twist-extension coupling induced by the helical structure of the cell wall has significant effect on the elastic behaviour of fibres. Boundary conditions, i.e. whether the fibres are allowed to twist or not, play an important role as well. Fibres that are constrained exhibit a stiffer response. The constrained boundary conditions are believed to best resemble the conditions in wood, composites or paper where fibres are surrounded by other fibres, embedded in a polymer matrix or constrained by fibre–fibre bonds, respectively.

It has been shown that the ultrastructure will influence the hygroexpansion behaviour of the cell wall in the same way as it influences its compliance behaviour (cf. Ref. [86] for wood based composites). No change of the expansion in a given direction can be achieved through varying the ultrastructure without concomitantly reducing or increasing the compliance in the direction of interest in the same proportion. Twisting is the dominating deformation mechanism when fibres are subjected to changes in moisture content. Better knowledge of influence of time, temperature and moisture content on the elastic properties of the wood polymers is required. Nevertheless, the method presented here may be used calculate deformation for low moisture content changes where changes in elastic constants are relatively small.

Stress analysis was carried out and the prediction of location of failure initiation in cylinders could qualitatively be linked to experimental observation of fracture in real fibres. For constrained (i.e. no twist allowed) wood fibres failure initiation in S2 may be expected at the S1-S2 interface as has also been observed in experiments (see Ref. [13]).

The combination of ultrastructural homogenisation and the coaxial cylinder model into a multiscalar modelling approach provides a potentially fruitful method to study effects of ultrastructural morphology on mechanical properties of wood fibres. However, experiments on single fibres as well as calculations on fibres with the irregular and more realistic geometry are indispensable for a better and more quantitative understanding of the hygroelastic behaviour of wood fibres.

Acknowledgments Financial support from the Wood Ultrastructure Research Centre (WURC) and the research cluster ''New Fibres for New Materials'' at STFI-Packforsk AB the is gratefully acknowledged.

Appendix A. Transformation of orthotropic hygroelastic constants

The 3D constitutive law for every layer k, written in matrix notation with respect to coordinate system (1, 2, 3) defined in Fig. 2, is

$$\{\varepsilon^*\}_k = [S^*]_k\{\sigma^*\}_k + \{\beta^*\}_k \Delta C \tag{A1}$$

where $[S^*]_k$ is the compliance matrix, $\{\varepsilon^*\}_k$ and $\{\sigma^*\}_k$ are the total strain and stress components, respectively, $\{\beta^*\}_k$ the hygroexpansion coefficients, which together with the change in moisture content ΔC give the strain due to changes in moisture content (in analogy with thermoelasticity). The hygroscopic strains are determined from a stress-free reference state, and the elastic properties are assumed to be constant. The compliance of an orthotropic material given in coordinates with the principal material axes is expressed in terms of the engineering elastic parameters like

$$[S^*]_k = \begin{bmatrix} 1/E_{11} & -\nu_{21}/E_{22} & -\nu_{31}/E_{33} & 0 & 0 & 0 \\ -\nu_{12}/E_{11} & 1/E_{22} & -\nu_{32}/E_{33} & 0 & 0 & 0 \\ -\nu_{13}/E_{11} & -\nu_{23}/E_{22} & 1/E_{33} & 0 & 0 & 0 \\ 0 & 0 & 0 & 1/G_{23} & 0 & 0 \\ 0 & 0 & 0 & 0 & 1/G_{13} & 0 \\ 0 & 0 & 0 & 0 & 0 & 1/G_{12} \end{bmatrix}_k \tag{A2}$$

The stresses $\{\sigma^*\}_k$ in each layer are expressed in terms of the layer strains as

$$\{\sigma^*\}_k = [C^*]_k\left(\{\varepsilon^*\}_k - \{\beta^*\}_k \Delta C\right) \tag{A3}$$

where the stiffness matrix $[C^*]_k$ is defined as

$$[C^*]_k = [S^*]_k^{-1} \tag{A4}$$

Because the main principal material axes of each layer are oriented at various angles, ϕ (i.e. MFA), to the fibre axis it is necessary to represent the constitutive law for all layers in the common global coordinate system (r, z, θ) shown in Fig. 2. The global stresses $\{\sigma\}_k$ and strains $\{\varepsilon\}_k$ are obtained by a rotation about the r-axis as following

$$\{\sigma\}_k = [R]_k\{\sigma^*\}_k \tag{A5}$$

and

$$\{\varepsilon\}_k = \left([R]_k^{-1}\right)^{\mathrm{t}}\{\varepsilon^*\}_k \tag{A6}$$

where t denotes matrix transpose and $[R]_k$ the transformation matrix is

$$[R]_k = \begin{bmatrix} 1 & 0 & 0 & 0 & 0 & 0 \\ 0 & \cos^2\varphi & \sin^2\varphi & 2\cos\varphi\sin\varphi & 0 & 0 \\ 0 & \sin^2\varphi & \cos^2\varphi & -2\cos\varphi\sin\varphi & 0 & 0 \\ 0 & -\cos\varphi\sin\varphi & \cos\varphi\sin\varphi & \cos^2\varphi - \sin^2\varphi & 0 & 0 \\ 0 & 0 & 0 & 0 & \cos\varphi & -\sin\varphi \\ 0 & 0 & 0 & 0 & \sin\varphi & \cos\varphi \end{bmatrix}_k \tag{A7}$$

Using Eqs. A3 and A6 the global stresses $\{\sigma\}_k$ in Eq. A5 can be expressed as

$$\{\sigma\}_k = [C]\{\varepsilon\}_k - \{\beta\}_k \Delta C \tag{A8}$$

where the global stiffness matrix of each layer $[C]_k$ is

$$[C]_k = [R]_k [C^*]_k [R]_k^{\mathrm{t}} \tag{A9}$$

and the stresses per unit moisture content change $\{\beta\}_k$ is

$$[\beta]_k = [C]_k \left([R]_k^{-1} \right)^{\mathrm{t}} \{\beta^*\}_k \tag{A10}$$

Appendix B. Identification of Tsai-Hill failure parameters

The failure parameters σ_{3u}, σ_{2u} and τ_{32u} in Eq. 31 can be determined from experimental data on single pulp fibres [59, 60]. From the previous description of the micro- and ultrastructure, it can be concluded that uncollapsed wood fibres can generally be regarded as filament wound composite tubes of various cross-section. The S2 layer is by far the thickest (Table 1) and can be considered to control the strength properties of the composites, therefore the presence of the other layers in the following treatment in disregarded. A common sample preparation for tensile testing of individual fibres involves pressing fibres during wet state into a collapsed form to simulate conditions of the papermaking process [59]. This means that the pulp fibre is like a flat collapsed box rather than a hollow tube, and can thus be treated as $\pm\phi$ angle ply laminate, $[\pm\phi]_T$, where ϕ is the MFA.

Under applied axial load an angle ply laminate will twist. However, in tensile testing of fibres, twist is prevented by mounting and fixation of the fibre ends. Therefore it is assumed that the fibre, i.e. a $\pm\phi$ laminate, is subjected to an axial load, resulting in an axial stress σ_z, and a moment, proportional to the axial load, of a magnitude such that a shear stress is induced in the cell wall that maintains the zero shear strain, i.e. no twist. Relation between global directions and the principal material direction are as defined in Fig. 2. The local stress state can be obtained with classical laminate theory and reads

$$\sigma_2 = \left(\sin^2\varphi + 2F(E_3, E_2, G_{32}, v_{32}, \varphi)\cos\varphi\sin\varphi\right)\sigma_z \tag{B1}$$

$$\sigma_3 = \left(\cos^2\varphi - 2F(E_3, E_2, G_{32}, v_{32}, \varphi)\cos\varphi\sin\varphi\right)\sigma_z \tag{B2}$$

$$\tau_{32} = -\left(\sin\varphi\cos\varphi - F(E_3, E_2, G_{32}, v_{32}, \varphi)\left(2\cos^2\varphi - 1\right)\right)\sigma_z \tag{B3}$$

where σ_3, σ_2 and σ_{23} are the principal stresses of the cell wall given as function of the applied axial stress, the elastic constants of the cell wall, E_2, E_3, G_{32}, v_{32}, entering function F, and the MFA, ϕ. The function F is given as follows

$$F = \frac{(2 + 2v_{32} - E_3/G_{32})\sin\varphi\cos^3\varphi - (2E_3/E_2 + 2v_{32} - E_3/G_{32})\sin^3\varphi\cos\varphi}{2(2 + 2E_3/E_2 + 4v_{32} - E_3/G_{32})\sin^2\varphi\cos^2\varphi + E_3/G_{32}(\cos^4\varphi + \cos^4\varphi)} \tag{B4}$$

Equations B1–B3 can be inserted into Eq. 31 that defines the Tsai-Hill criterion and a relationship between applied stress, Tsai-Hill parameters and the MFA is obtained as

$$\sigma_z = \left(\left(\frac{\alpha_3}{\sigma_{3u}}\right)^2 + \left(\frac{\alpha_2}{\sigma_{2u}}\right)^2 + \left(\frac{\alpha_{32}}{\tau_{32u}}\right)^2 \right)^{-1/2} \tag{B5}$$

where

$$\alpha_2 = \left(\sin^2\varphi + 2F\cos\varphi\sin\varphi\right)^2 \tag{B6}$$

$$\alpha_3 = \left(\cos^2\varphi - 2F\cos\varphi\sin\varphi\right)^2 - \left(\cos^2\varphi - 2F\cos\varphi\sin\varphi\right)\left(\sin^2\varphi + 2F\cos\varphi\sin\varphi\right) \tag{B7}$$

$$\alpha_{32} = \left(\sin\varphi\cos\varphi - F\left(2\cos^2\varphi - 1\right)\right)^2 \tag{B8}$$

Equation B5 can be fitted to any suitable experimental correlation between the tensile strength and MFA in S2 to determine the different failure parameters.

References

1. Neagu RC, Gamstedt EK, Berthold F (2006) J Compos Mater 40:663
2. Tarn JQ, Wang YM (2001) Int J Solids Struct 38:9053
3. Tarn J-Q (2002) Int J Solids Struct 39:5143
4. Tarn JQ (2002) Int J Solids Struct 39:5157
5. Jolicoeur C, Cardou A (1994) J Eng Mech-ASCE 120:2556
6. Tang RC (1972) Wood Fiber Sci 3:210
7. Gillis PP, Mark RE (1973) Cell Chem Technol 7:209
8. Davies GC, Bruce DM (1997) J Mater Sci 32:5424
9. Sutcu M (1992) Int J Solids Struct 29:197
10. Hill R (1965) J Mech Phys Solids 13:189
11. Gillis PP (1970) Fibre Sci Technol 2:193
12. Neagu RC (2006) Report. KTH Solid Mechanics, Royal Institute of Technology, Stockholm, Sweden, p 83
13. Mark RE (1967) Cell wall mechanics of tracheids. Yale University Press, New Haven, p 241
14. Schniewind AP, Barrett JD (1969) Wood Fiber Sci 1:205
15. Mark RE, Gillis PP (1970) Wood Fiber Sci 2:79
16. Mark RE, Gillis PP (1973) TAPPI 56:164
17. Page DH, El-Hosseiny F, Winkler K, Lancaster APS (1977) TAPPI 60:114
18. Salmén L, de Ruvo A (1985) Wood Fiber Sci 1985:336
19. Salmén L, Kolseth P, de Ruvo A (1985) J Pulp Pap Sci 11:102
20. Persson K (2000) Doctoral Thesis, Department of Mechanics and Materials, Structural Mechanics. LTH, Lund University, Lund, Sweden, p 213
21. Bergander A, Salmen L (2002) J Mater Sci 37:151. DOI: 10.1023/A:1013115925679
22. Barber NF (1968) Holzforschung 22:97
23. Barrett JD, Schniewind AP (1973) Wood Fiber Sci 5:215
24. Gassan J, Chate A, Bledzki AK (2001) J Mater Sci 36:3715
25. Lekhnitskii SG (1981) Theory of elasticity of an anisotropic body. Mir, Moscow
26. Wardrop AB, Preston RD (1947) Nature 160:911
27. Harada H, Côté WA Jr (1985) In: Higuchi T (ed) Biosynthesis and biodegradation of wood components. Academic Press Inc., Orlando, FL, USA, p 679
28. Brändström J (2002) Doctoral thesis, Department of Wood Science, Acta Universitatis agriculturae Sueciae, Silvestria vol 237 SLU, Uppsala, p 39
29. Panshin AJ, de Zeeuw C (1980) Textbook of wood technology. McGraw-Hill, New York
30. Fengel D (1970) TAPPI 53:497
31. Fahlén J, Salmén L (2003) J Mater Sci 38:119
32. Salmén L, Olsson AM (1998) J Pulp Pap Sci 24:99
33. Kerr AJ, Goring DAI (1975) Cell Chem Technol 9:563
34. Meylan BA, Butterfield BG (1978) Wood Sci Technol 12:219
35. Brändström J, Bardage SL, Daniel G, Nilsson T (2003) IAWA J 24:27
36. Bergander A, Brändström J, Daniel G, Salmén L (2002) J Wood Sci 48:255
37. Abe H, Ohtani J, Fukazawa K (1992) IAWA Bull New Ser 13:411
38. Abe H, Funada R (2005) IAWA J 26:161
39. Abe H, Ohtani J, Fukazawa K (1991) IAWA Bull New Ser 12:431
40. Fengel D (1972) Holzforschung 26:1
41. Fernando D, Daniel G (2004) Nord Pulp Pap Res J 19:278
42. Brändström J (2001) IAWA J 22:333
43. Fengel D (1969) Wood Sci Technol 3:203
44. Fengel D, Stoll M (1973) Holzforschung 27:1
45. Kollman FFP, Côté WA (1968) Principles of wood science and technology. 1. Solid wood. Springer-Verlag, Berlin, Germany
46. Keckes J, Burgert I, Fruhmann K, Muller M, Kolln K, Hamilton M, Burghammer M, Roth SV, Stanzl-Tschegg S, Fratzl P (2003) Nature Mater 2:810
47. Booker RE, Sell J (1998) Holz Roh Werkst 56:1
48. Åkerholm M, Salmén L (2003) Holzforschung 57:459
49. Sakurada I, Nukushina Y, Ito T (1962) J Polym Sci 57:651
50. Cousins WJ (1976) Wood Sci Technol 10:9
51. Cousins WJ (1978) Wood Sci Technol 12:161
52. Tashiro K, Kobayashi M (1991) Polymer 32:1516
53. Nakamura KI, Wada M, Kuga S, Okano T (2004) J Polym Sci Pol Phys 42:1206
54. Cave ID (1978) Wood Sci Technol 12:75
55. Neumann S, Marom G (1986) J Mater Sci 21:26
56. Bahar LY (1975) J Franklin I 299:33
57. Wang J, Fang S (1999) Mech Res Commun 26:673
58. Agarwal BD, Broutman LJ (1990) Analysis and performance of fiber composites. John Wiley & Sons, Inc., New York
59. El-Hosseiny F, Page DH (1975) Fibre Sci Technol 8:21
60. Page DH, El-Hosseiny F (1983) J Pulp Pap Sci 9:TR 99
61. Christensen RM (2001) In: Aref H, Philips JW (eds) Mechanics for a new millenium. Kluwer Academic Publishers, Neherlands, p 25
62. Hashin Z, Rosen BW (1964) J Appl Mech 31:223
63. Hashin Z (1979) J Appl Mech 46:543
64. Christensen RM, Lo KH (1979) J Mech Phys Solids 27:315
65. Hervé E, Zaoui A (1995) Int J Eng Sci 33:1419
66. Hashin Z (1983) J Appl Mech 50:481
67. Marklund E (2005) Licentiate thesis, Department of Applied Physics and Mechanical Engineering, Division of Polymer Engineering. Luleå University of Technology, Luleå, Sweden
68. Chouchaoui CS, Ochoa OO (1999) Compos Struct 44:221
69. Xia M, Takayanagi H, Kemmochi K (2001) Compos Struct 53:483
70. Byron Pipes R, Hubert P (2002) Compos Sci Technol 62:419
71. Byron Pipes R, Hubert P (2003) Compos Sci Technol 63:1571
72. Neagu RC, Gamstedt EK, Lindström M (2006) In: Salmén L (ed) 5th Plant biomechanics conference. STFI-Packforsk AB, Stockholm, Sweden, in press
73. Jayne BA (1959) TAPPI 42:461
74. Jentzen CA (1964) TAPPI 47:412
75. Leopold B (1966) TAPPI 49:315
76. Spiegelberg HL (1966) TAPPI 49:388
77. Kersavage PC (1973) Wood Fiber Sci 5:105
78. Groom LH, Mott L, Shaler SM (2002) Wood Fiber Sci 34:14
79. Mott L, Groom LH, Shaler SM (2002) Wood Fiber Sci 34:221
80. Duncker B, Nordman L (1968) Sven Papperstidn 71:165
81. de Ruvo A, Lundberg R, Martin-Löf S, Söremark C (1976) In: Bolam F (ed) The fundamental properties of paper related to its

uses, Transactions of the symposium 1973. British Paper and Board Makers' Association, London, p 785
82. Kolseth P, Ehrnrooth EML (1986) In: Bristow JA, Kolseth P (eds) Paper structure and properties. Marcel Dekker Inc., New York, p 27
83. Wallström L, Lindberg KAH, Johansson I (1995) Holz Roh Werkst 53:87
84. Meylan BA (1972) Wood Sci Technol 6:293
85. Schulgasser K, Witztum A (2004) J Theor Biol 230:281
86. Schulgasser K (1987) In: Proceedings of the international paper physics conference, Quebec, edited by p 53
87. Wilhelmsson D, Neagu RC, Bardage SL, Gamstedt EK (2006) In: Salmén L (ed) 5th Plant biomechanics conference. STFI-Packforsk AB, Stcockholm, Sweden, in press